Neurexin/Neuroligin Interaction Kinetics Characterized by Counting Single Cell-Surface Attached Quantum Dots

Edouard Saint-Michel, Grégory Giannone, Daniel Choquet, and Olivier Thoumine*
Physiologie Cellulaire de la synapse, Centre National de la Recherche Scientifique and University of Bordeaux, Bordeaux, France

ABSTRACT We report what to our knowledge is a new method to characterize kinetic rates between cell-surface-attached adhesion molecules. Cells expressing specific membrane receptors are surface-labeled with quantum dots coated with their respective ligands. The progressive diminution in the total number of surface-diffusing quantum dots tracked over time collectively reflects intrinsic ligand/receptor interaction kinetics. The probability of quantum dot detachment is modeled using a stochastic analysis of bond formation and dissociation, with a small number of ligand/receptor pairs, resulting in a set of coupled differential equations that are solved numerically. Comparison with the experimental data provides an estimation of the kinetic rates, together with the mean number of ligands per quantum dot, as three adjustable parameters. We validate this approach by studying the calcium-dependent neurexin/neuroligin interaction, which plays an important role in synapse formation. Using primary neurons expressing neuroligin-1 and quantum dots coated with purified neurexin-1β, we determine the kinetic rates between these two binding partners and compare them with data obtained using other techniques. Using specific molecular constructs, we also provide interesting information about the effects of neurexin and neuroligin dimerization on the kinetic rates. As it stands, this simple technique should be applicable to many types of biological ligand/receptor pairs.

INTRODUCTION

Adhesion between living cells is a fundamental process in biology. Cell-cell recognition is mediated by specific ligand/receptor molecules expressed on cell surfaces, which can form selective bonds through key-lock structural interfaces. The initiation and duration of an adhesive contact intimately relies on the intrinsic properties of the ligand/receptor assembly, in particular the on/off reaction rates. To estimate these parameters, two types of approach are currently available: 1), measurements on populations of ligand/receptor pairs in combination with deterministic chemical reaction models, e.g., using radioactive or fluorescent labeling (1,2), or detection of molecular layers by optical techniques (3,4) or surface plasmon resonance (5); or 2), identification and statistical analysis of individual ligand/receptor bonds, e.g., using the flow chamber (6), atomic force microscopy (7), micropipette manipulation (8,9), optical tweezers (10), or single-molecule fluorescence imaging (11).

Lifetimes of bonds between biological molecules span several orders of magnitude, from <1 s for selectins and cadherins (6–8) to tens of minutes or hours for antibody-antigen and avidin-biotin interactions (9). Although some assays can accommodate the presence of cells, most studies were performed using purified ligands and receptors grafted to artificial surfaces. However, the way in which the protein attaches to surfaces may affect its binding properties. Also, analysis of individual binding and unbinding events often requires tedious data analysis.

We propose here an alternative approach using quantum dots (Qdots) coated with purified ligands to label individual receptors. The idea is to follow the detachment of single Qdots from the cell surface, which should reflect the rupture of ligand-receptor bonds. To demonstrate the feasibility of the technique, we focused on neurexin/neuroligin complexes, which form calcium-dependent interactions of equilibrium constants in the nanomolar range (5,12,13) and play a critical role in bridging together axons and dendrites during synaptogenesis (14). Specifically, we concentrate on the interaction between the membrane-associated adhesion molecules neurexin-1β (Nrx1β) and neuroligin-1 (Nlg1), involved in the formation of excitatory synapses (15,16). Using fluorescence-time-lapse imaging and image analysis, we demonstrate the selective detachment of Nrx1β-coated quantum dots from the surface of primary neurons expressing Nlg1. We interpret the experimental data with a kinetic model of ligand/receptor bond formation and dissociation, yielding the kinetic rates of the neurexin/neuroligin interaction, as well as an estimate of the small number of neurexin ligands grafted on the nanoparticles.

MATERIALS AND METHODS

Molecular constructs and reagents

The N-terminal HA-tagged murine neuroligin-1 construct (Nlg1-HA), and the pcDNA neomycin murine neurexin-1β ectodomain lacking splice insertion 4 and fused to the constant fragment of human IgG (Nrx1β-Fc), were generous gifts from P. Scheiffele (15) (Biozentrum, Basel, Germany). An Nlg1 construct (Nlg1-monomer) in which amino acids E584 and L585 in the Nlg1-HA gene were replaced by alanine residues was generated by site-directed mutagenesis (Quikchange IIXL kit, Stratagene, La Jolla, CA). These mutations are targeted to an α-helix in the acetylcholine esterase-like

Submitted December 26, 2008, and accepted for publication April 27, 2009.

*Correspondence: olivier.thoumine@pcs.u-bordeaux2.fr

Editor: Michael Edidin.

0006-3495/09/07/0480/10 $2.00

doi: 10.1016/j.bpj.2009.04.044

ectodomain involved in the formation of constitutive Nlg1 dimers through coiled-coil formation (15). These mutant Nlg1 molecules, unable to dimerize, still bind Nrx1β but can no longer induce clustering of adhesive zones or functional presynapse assembly (15). The Nrx1β-Fc plasmid was subcloned between sites *Hin*dIII/XhoI in pcDNAhygro(+) vector to select a stable hygromycin-resistant HEK cell line producing Nrx1β-Fc. Recombinant Nrx1β-Fc protein was purified from ~1 L of conditioned medium on a protein G affinity column (17). The final concentration of 1.0 mg/ml was estimated by Bradford assay (MicroBCA kit, Pierce, Rockford, IL). SDS-PAGE and immunoblotting with a mouse antibody against human Fc (Jackson Immunoresearch, West Grove, PA) was performed as described (2). The Fc fusion proteins spontaneously assemble into dimers due to the presence of disulfide bonds in the Fc fragment (18) (Fig. 1 *b*). We also produced monomeric Nrx1β-Fc by treating the purified protein preparation with 10 mM dithiothreitol (DTT) for 30 min at room temperature, then centrifuging at 14,000 rpm for 2 h in Centricon filtering units (Millipore, Billerica, MA). Purified human Fc (Jackson Immunoresearch) was conjugated to Cy3 fluorophores in a 1:1 stoichiometry using a commercial coupling kit (Amersham, Fairfield, CT).

Cell culture and transfection

Dissociated hippocampal neurons from E18 rat embryos were plated on 18-mm polylysine-coated glass coverslips at a density of 10,000 cells/cm^2 in minimal essential medium containing 10% horse serum (Gibco, Billings, MT) for 3 h, then cultured in neurobasal medium supplemented with B27 on a layer of glial cells, as described (2). Neurons were cotransfected at 3 or 4 days in vitro with green fluorescent protein (GFP) and Nlg1-HA or Nlg1-monomer using Effectene (Qiagen, Venlo, The Netherlands) and processed 3–4 days later.

Quantum dot preparation

We incubated 3 μl of 655-nm Qdots (1 μM stock solution, Invitrogen) conjugated with goat (Fab')$_2$ anti-human or anti-rat IgG with, respectively, 0.5 μl of 0.5 mg/ml monomeric Nrx1β-Fc (1 μM), 0.5 μl of 1 mg/ml dimeric Nrx1β-Fc (1 μM) or 3 μl of 100 μg/ml (0.5 μM) rat anti-HA antibodies (Roche) in 21 μl phosphate-buffered saline for 20 min, then blocked with 3 μl of a 10% casein solution (Vector Labs) and kept on ice (Fig. 1 *a*). To quantify the number of binding sites per Qdot, 3 μl anti-human conjugated Qdots were coated with 0.3 μl of 1 mg/ml Cy3-labeled human Fc (1 μM), then spread at a 1:10,000 dilution in phosphate-buffered saline on polylysine-coated glass coverslips and observed on a Nikon microscope having filter sets with minimal bleed-through between Cy3 and Qdot channels (Fig. 1 *c*).

Imaging quantum dot mobility and detachment

Cells were incubated with 5 μl Qdot suspension in 1 ml culture medium containing 1% globulin-free bovine serum albumin (Sigma, St. Louis, MO) for 10 min at 37°C, and rinsed three times before mounting in 200 μl Tyrode

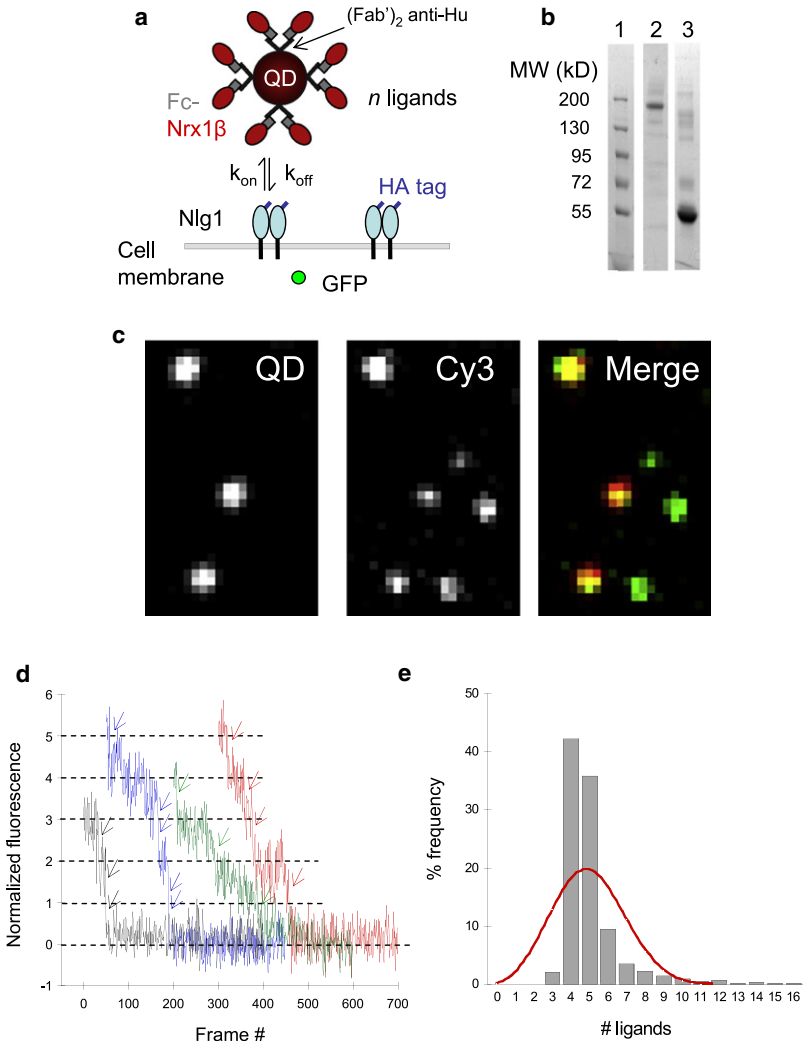

FIGURE 1 Experimental design and quantum dot coating. (*a*) Diagram of the molecular interactions. (*b*) Coomassie staining of purified Nrx1β-Fc samples run on an SDS polyacrylamide gel under nonreducing conditions. *Lane 1*, molecular mass standards (kD); *lane 2*, raw Nrx1β-Fc preparation, showing high-molecular-weight species, presumably dimers; *lane 3,* the same sample pretreated with DTT to produce monomeric Nrx1β-Fc, which migrates at the predicted molecular mass of 55 kD. Note the purity of the sample preparations. Parallel immunoblots of the same gels probed with an anti-human Fc antibody reveal bands at the same molecular masses (not shown). (*c*) Qdots coated with Cy3-conjugated human Fc were spread on glass coverslips and images were taken in both channels. The maximum projection of 400 images taken at 10 Hz was computed to detect all Qdots in the field of view (even blinking ones), and to take into account the unbleached Cy3 values. Note that the Cy3 signal colocalizes with Qdots, and that some Cy3-Fc spots are bound to the coverglass, indicating that not all Fc-Cy3 molecules are associated with Qdots. (*d*) Examples of photobleaching curves for Fc-Cy3 bound to Qdots. Note the appearance of unitary steps (*arrows*) interpreted as the photobleaching of individual Fc-Cy3 fluorophores. Curves were normalized by the intensity difference characterizing these steps (i.e., 780 gray levels on a 16-bit camera). (*e*) Distribution of Fc-Cy3 intensities at Qdots, normalized by the unitary bleaching value, for 3875 Qdots on 20 different fields of view. The red curve is a binomial distribution with average $\langle n \rangle = 5$ and maximum $m = 16$. Both data sets indicate that Qdots are coated with just a few Fc molecules.

solution (120 mM NaCl, 5 mM KCl, 2 mM $MgCl_2$, 2 mM $CaCl_2$, 25 mM HEPES, and 30 mM D-Glucose, pH 7.4) on a fluorescence microscope (IX70, Olympus, Melville, NY). Qdots were visualized using a filter set from Chroma (BP 460-490 nm excitation filter, 500 nm dichroic mirror, and 655/20 nm emission filter; Rockingham, VT), and a cooled digital camera (Quantem, Roper Scientific, Trenton, NJ) driven by MetaMorph (Universal Imaging, Washington, DC.). Cells were screened based on GFP fluorescence, and the coexpression of Nlg1-HA was detected by the presence of anti-HA- or Nrx1β-Fc-coated Qdots. We selected cells with, typically, 200–500 Qdots on an 80 μm × 80 μm camera field, corresponding to a density in the range of 0.1–0.8 Qdots/μm^2 of cell surface area. Then, images in the Qdot channel were taken every 2 s for 30 min, resulting in essentially no photobleaching. In competition experiments, neurons labeled with monomeric Nrx1β-Fc-coated Qdots were treated 5 min after the start of the recording with 10 mM EGTA in Tyrode solution lacking Ca and Mg, or 50 μg/ml dimeric Nrx1β-Fc, using an open chamber and a peristaltic perfusion system. To detect the instantaneous detachment of monomeric Nrx1β-Fc coated Qdots, the image acquisition rate was increased to 50 Hz for 3 min, right after EGTA treatment.

Tracking and counting of quantum dots by image analysis

Qdots images were processed using the multidimensional analysis module based on wavelet segmentation and running on Metamorph (19). This program allows identification of Qdots as individual objects and attributes to each object a gray value based on its time of appearance within an image stack. For fast acquisitions aiming to show individual Qdot detachment and to measure lateral mobility, Qdot positions were tracked and reconnected using home-made algorithms written in MATLAB software (The MathWorks, Natick, MA), yielding 2D trajectories (19). Fitting the initial slope of the mean-square displacement function over time yields the instantaneous diffusion coefficient (20). For global detachment experiments, the number of Qdots present in the image is obtained simply by applying a threshold of 1 on the multidimensional analysis image, and a routine was written within Metamorph to rapidly read a whole image stack and extract a data log file. We focused on the mobile Qdot population by discarding immobile Qdots using either subtraction between subsequent images, or subtraction from each image of the arithmetic average made on the whole stack (which reveals essentially immobile Qdots). By normalizing with respect to Qdot number at the beginning of the observation, one gets rid of variations in Qdot labeling due to cell-to-cell heterogeneities in Nlg1 expression levels.

Estimation of the number of ligands per Qdot

The hydrodynamic diameter of water-soluble polymer-coated Qdots, similar to commercial ones, was estimated by fluorescence correlation spectroscopy to be in the range 28–32 nm (21,22). If we consider that Nrx1β-Fc (50 kD) has approximately the same size as globular actin (5 nm), one can fit a maximum number of $m = 16$ ligands at saturation, corresponding to a coverage density of 1.3×10^4 ligands/μm^2. This theoretical estimate fits with physicochemical determinations of ligand number for streptavidin-coated Qdots, i.e., 10–20 for the 655-nm Qdots we used (23,24). Because of dilution, we assume that after coating, each Qdot bears a smaller number, n, of Nrx1β-Fc ligands (Fig. 1 *a*). Given size dispersion in the Qdot batch and coating heterogeneity, this number is susceptible to slight variation between different QDots, introducing some scatter in n. To estimate the distribution of n, we used purified human Fc conjugated to single Cy3 fluorophores, coated to Qdots at the same dilution as Nrx1β-Fc. The Cy3 signal at Qdot locations was found to decrease in multiple discrete steps with a characteristic intensity value (Fig. 1 *d*). This was interpreted as the successive photobleaching of individual Fc-Cy3 molecules, indicating the presence of just a few Fc molecules per Qdot. The initial (prebleach) Cy3 intensity on each QDot was then divided by this unitary value, giving the overall distribution of Cy3-Fc molecules per Qdot (Fig. 1 *e*). This surprisingly sharp experimental histogram was fitted by a binomial distribution centered on the average $\langle n \rangle = 5$, assuming a maximum value of $m = 16$ binding sites (Fig. 1 *e*).

Theoretical model and simulations

Hypotheses and choice of parameters

The interaction between Nrx1β ligands conjugated to Qdots and Nlg1 receptors expressed at the cell surface was taken as a first-order chemical reaction, with apparent association rate k_{on} (s^{-1}) and dissociation rate, k_{off} (s^{-1}), both treated as constant. k_{on} may a priori depend on receptor density and lateral diffusion (25–27). Assuming an Nlg1 receptor density of ~500/μm^2, as quantified previously for N-cadherin and Immunoglobulin cell adhesion molecules (IgCAMs) in primary hippocampal neurons using similar transfection conditions (2,20), and a cell surface area of ~3000 μm^2, one gets an estimate of 1.5×10^6 receptors/neuron. Given a maximal number of 1000 Qdots bound per cell and an upper value of 10 conjugated ligands per Qdot, the maximal number of ligand-bound receptors/cell is 10^4. Thus, the fraction of occupied receptors (<1%) is negligible, and the free receptor density can be taken as constant (except in competition experiments using soluble Nrx1β to artificially reduce free receptor availability). We will retrospectively confirm this hypothesis by plotting the effect of receptor density on k_{on}. The ligand/receptor association rate is also unlikely to be limited by membrane diffusion, for at least three reasons: 1), there is a large excess of free receptors; 2), Qdots explore the overall cell surface area by diffusion; 3), because Qdots are small, receptors are unlikely to experience steric hindrance for diffusing to the vicinity of a ligand. Accordingly, the recruitment rate of IgCAMs expressed at the surface of neurons by antibody-coated microspheres was shown to weakly depend on lateral diffusion, albeit in a geometrically more confined environment (20). In such a reaction-limited regime, k_{off} should not be affected by bond number (26). However, k_{off} may indirectly depend on bond number if mechanical force is applied to an ensemble of bonds acting in parallel. Indeed, strain is known to accelerate the frequency of bond dissociation in an exponential manner (9,25). Here, the dissociation force is only that of thermal motion, i.e., essentially zero, thus k_{off} should be independent of the number of bonds.

Model formulation

Let us start with the description of a single Qdot bearing n ligands. The probability that a number i (ranging from 0 to n) of ligand/receptor pairs are formed at time t, is written $P_i(t)$. The transitions between nearest neighbors (states $i - 1$, i, and $i + 1$) were written as described previously (28,29):

$$\text{For } i > 1 \; dP_i/dt = k_{on} P_{i-1} - \left(k_{on} + ik_{off}\right) P_i + (i+1)k_{off} P_{i+1}. \quad (1)$$

We did not allow the transition $0 \rightarrow 1$, which would correspond to a novel adhesion event, resulting in specific equations for P_1 and P_0:

$$dP_1/dt = -\left(k_{on} + k_{off}\right)P_1 + 2k_{off}P_2 \quad (2)$$

$$\text{and } dP_0/dt = k_{off}P_1. \quad (3)$$

We assumed that at the start of the recording (time 0), each individual ligand on the particle is at equilibrium binding, resulting in a binomial distribution of bonds:

$$P_i(0) = (n, i)\, k^i\, (1-k)^{n-I}, \quad (4)$$

where the binomial coefficient is $(n, i) = n!/[i!(n-i)!]$, and $\kappa = 1/(1 + k_{off}/k_{on})$ is the probability of the free-to-bound transition for a single ligand/receptor pair (10). This set of coupled differential equations was solved numerically using the Mathematica software (Wolfram Research, Champaign, IL). The probability that a Qdot bearing n ligands will remain attached

to the cell surface, $P_a(n)$, was then taken as the probability of having at least one ligand/receptor bond:

$$P_a(n) = \sum_{i=1}^{n} P_i = 1 - P_0. \quad (5)$$

Then, to predict the behavior of a population of Qdots with nonuniform coating, each individual probability was weighted by its respective occurrence, according to a binomial distribution of n, i.e.

$$P_a = \sum_{n=1}^{m} (m, n) [\langle n \rangle / m]^n [1 - \langle n \rangle / m]^{m-n} P_a(n), \quad (6)$$

where m is the maximal number of binding sites per Qdot (in practice, $m = 16$).

Simulations and fitting

We give examples of simulated detachment curves for several sets of parameters (see Fig. S1, *a–c*, in the Supporting Material). We chose $\langle n \rangle$ values in the range 2–10, and k_{off} centered around 0.9 min^{-1}, a value from the literature (5). Finally, we take k_{on} in the range 1–10 min^{-1} to yield curves resembling those obtained experimentally over a time course of 30 min. To fit the experimental Qdot attachment probability data, a series of computer simulations was carried out by varying k_{on} for different $\langle n \rangle$ values while maintaining k_{off} at 0.9 min^{-1}. For each experimental Qdot detachment curve, the sum of squared residuals between experimental and theoretical attachment probability values was calculated over all time points (30). The set of k_{on} and $\langle n \rangle$ values yielding the smallest sum of squared residuals was chosen (Fig. S1 *d*).

RESULTS

Cellular and molecular tools

To probe the kinetics of interaction between Nrx1β and cell-surface-associated Nlg1, we used the following protocol. On the receptor side, primary hippocampal neurons were cotransfected at 6–7 days in vitro (DIV) with Nlg1-HA and GFP used as a live reporter. Nlg1 is a single-pass transmembrane molecule that assembles into a constitutive dimer through coiled coils between α-helices situated in the ectodomain (15). To assess the effect of receptor dimerization on the binding properties, we produced an Nlg1 receptor with two successive point mutations (E584A/L585A) in the α-helix region preventing dimer assembly (15), which we called ''Nlg1-monomer''. On the ligand side, 655 nm commercially available Quantum dots (31) conjugated with $(Fab')_2$ anti-human IgG were coated to equimolar amounts of purified recombinant Nrx1β fused to the Fc fragment of human IgG (Nrx1β-Fc) (Fig. 1 *a*). Nrx1β-Fc migrated as a multimer in polyacrylamide gels under nonreducing conditions, because of disulfide bonds formed between the two Fc regions (Fig. 1 *b*). To assess the effect of ligand multivalency, we produced a monomeric form of Nrx1β-Fc by chemical treatment with a reducing agent (DTT). The reduced protein migrated at the expected molecular mass of 55 kD, whereas the supposedly dimeric molecule had an apparent molecular mass around 150 kD, possibly due to an extended 3D conformation (Fig. 1 *b*). An alternative hypothesis is that the 150-kD band represents higher-order Nrx1β-Fc oligomers (trimers or even tetramers), since in anti-Fc immunoblots, a weak band appears at 110 kD, the expected size of dimers (not shown). Why these multimers should form is unclear, since there is no evidence for disulfide bond-dependent dimerization of Nrx1β (13,14). In the remainder of this article, we will refer to these proteins as Nrx1β-Fc dimers, knowing that there is a small doubt about their actual composition. As a reference robust interaction, we used Qdots coated with anti-HA antibodies, which also recognized transfected Nlg1 molecules bearing an HA tag in their extracellular domain (Fig. 1 *a*). Neurons were taken at 8–10 DIV, a time window of active synaptogenesis in these cultures (16). They were incubated with a fairly high concentration of the Qdot suspension (5 nM) for 10 min and rinsed before observation under an epifluorescence microscope.

Quantum dot behavior at the cell surface

Qdots bound numerously to the surface of neurons expressing Nlg1 and mildly to endogenous neuroligins on untransfected neurons (Fig. 2, *a–c*), demonstrating specific Nrx1β/Nlg1 interaction. Two equally abundant Qdot populations were observed: 1), freely diffusive Qdots exploring large distances on dendrites (Fig. 2, *c* and *d*); and 2), immobile Qdots (Fig. 2 *e*), which were interpreted as being either internalized in endocytic compartments, or trapped in high-order aggregates by stationary cytoskeletal elements (16). This immobile population (Fig. 2 *g*) was discarded from further analysis by either subtracting the number obtained on the average image (Fig. 2 *e*) or subtracting images two by two to count only the mobile Qdots (Fig. 2 *f*), with similar results. When filmed at a high camera acquisition rate (20 Hz), we observed the occasional detachment of Nrx1β-Fc coated Qdots, which quickly diffused into the extracellular medium (Fig. 3 and Movie S1). Accordingly, the detachment was associated with a rapid and ~100-fold increase in diffusion coefficient (Fig. 3 *d*). These events were attributed to the rupture of ligand-receptor bonds at the level of the Nrx1β/Nlg1 interface, since the coupling of the adhesive ligand to the Qdot via an antibody-Fc link is very stable (see next paragraph). One could in theory count the occurrence of these rupture events to get the unbinding frequency, but this would be extremely time-consuming.

Specific long-term detachment of Nrx1β-coated quantum dots

We found that a more straightforward approach was to film at lower frequency (0.5 Hz) and simply count the number of mobile Qdots bound to the cell surface on a large field of view, and for long times (Fig. 4 *a*). The goal was no longer to resolve individual trajectories, as classically done to measure diffusion properties (20), but to detect a long-term detachment rate. There are several intrinsic sources of noise

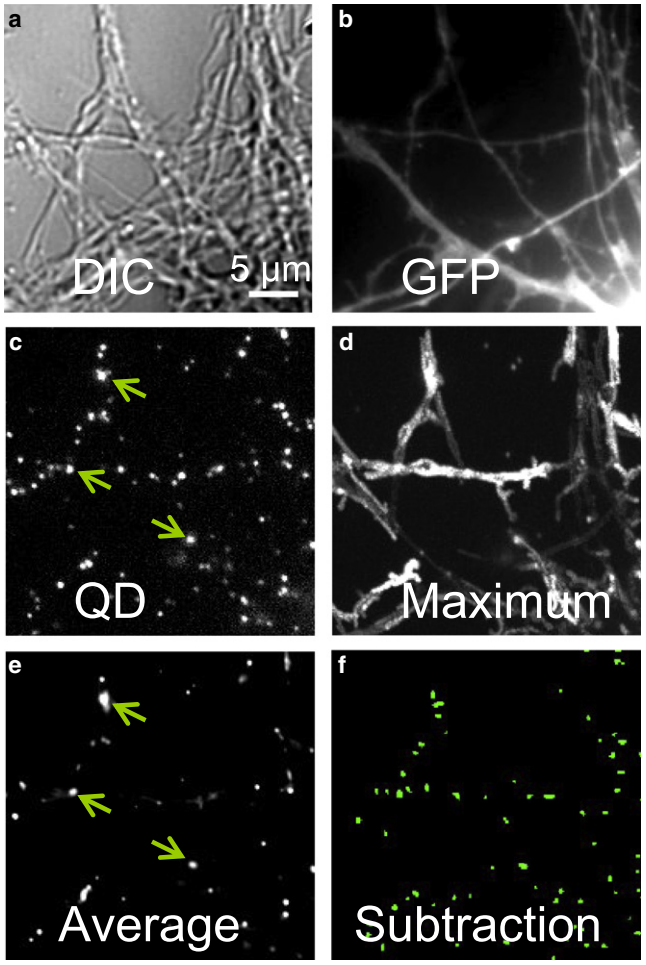

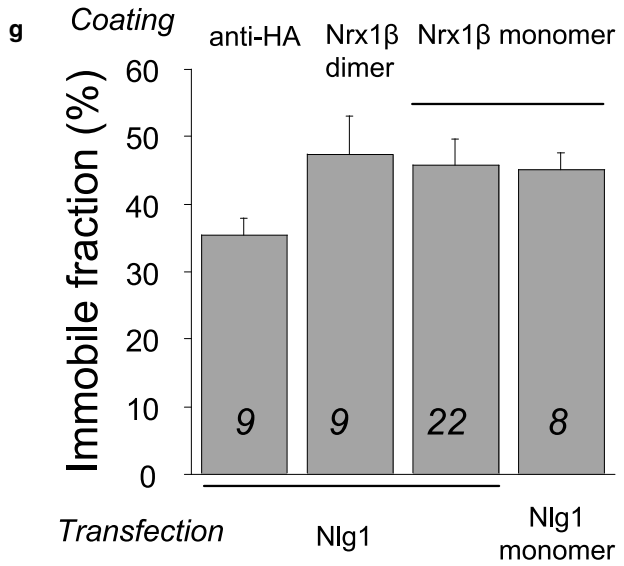

FIGURE 2 Binding and surface diffusion of Nrx1β-coated Quantum dots. (*a*) Differential interference contrast image. (*b*) GFP image of a 7-DIV neuron cotransfected with Nlg1-HA and GFP. (*c*) Raw static image of Nrx1β-Fc-coated Qdots bound to the surface of neurites. (*d*) Maximum image showing the cumulated trajectories of Qdots over 30 min. Note that Qdots nicely label transfected cells. (*e*) Stack average revealing the immobile Qdots. (*f*) Subtraction of two subsequent images, revealing essentially mobile Qdots. The image is further segmented and submitted to a threshold to allow clear separation and counting of individual Qdots. (*g*) Plot of the immobile fraction for all conditions. The number of cells examined is indicated in italics on each column.

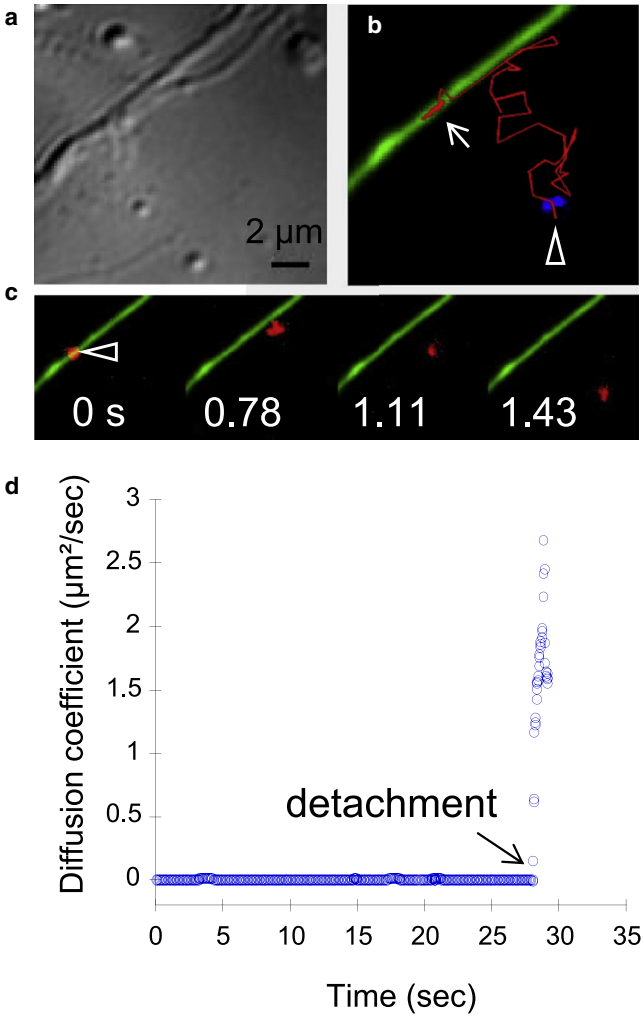

FIGURE 3 Images showing the detachment of an individual Nrx1β-Fc-coated Qdot in the presence of EGTA. (*a*) Differential interference contrast image. (*b*) Superimposition of the GFP-expressing neurite (*green*), the Qdot trajectory (*red*), and the Qdot right before it escapes the focal plane (*blue*, *arrowhead*). The arrow indicates the 30-s trajectory followed by the Qdot on the neurite surface before detachment and escape into the extracellular medium. The last part of the trajectory lasted 1.5 s before the Qdot escaped detection. (*c*) Sequential images of Qdot detachment (time indicated in seconds). (*d*) Plot of the diffusion coefficient over time.

in the assay, including repeated blinking of Qdots (sometimes for long periods of time), photobleach, and some Qdots entering and leaving the field of view by diffusion. In addition, collisions and potential aggregation between Qdots, as well as variations in cell height, contribute some uncertainty regarding the detection of individual Qdots. Altogether, these effects experimentally translate into $\pm 10\%$ fluctuations

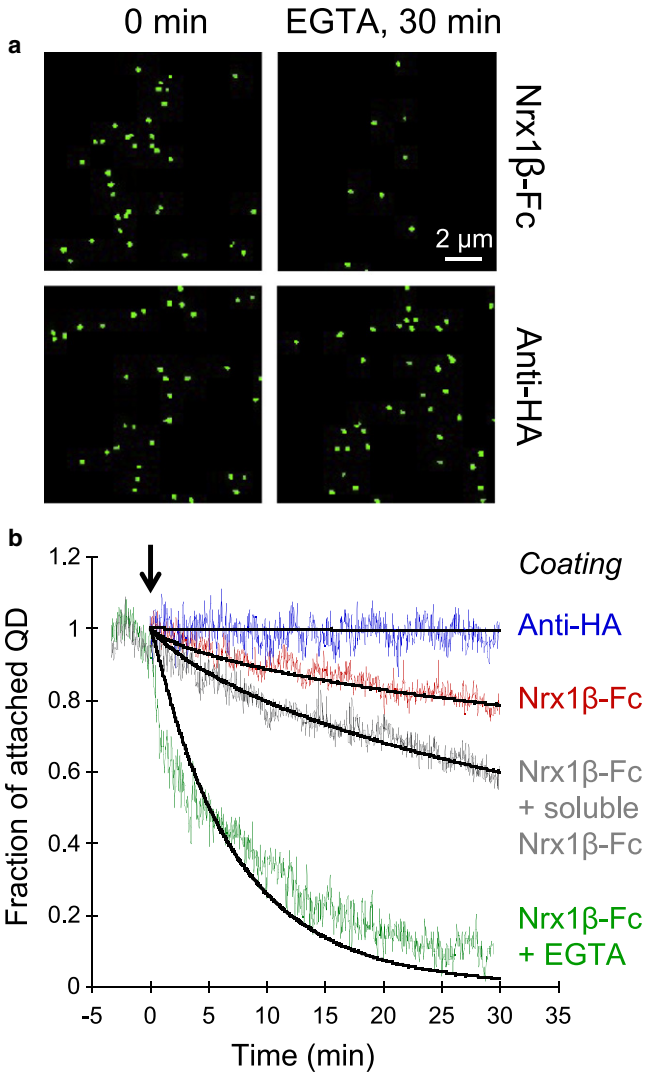

FIGURE 4 Counting the global detachment of Nrx-1β-coated Qdots from Nlg1-expressing cells. (*a*) Cell region labeled with Nrx1β-conjugated Qdots (*upper*) or anti-HA-coated Qdots (*lower*), before (*left*) or after (*right*) treatment with 10 mM EGTA. Raw Qdot images were treated by wavelet-based image analysis, allowing clear identification of individual particles. Note a dramatic reduction in the number of surface-attached Qdots for the Nrx1β-Fc ligand (from 36 to 8), but not for the anti-HA condition (41 before and 38 after EGTA treatment). (*b*) Graph showing the number of Qdots bound to Nlg1-HA-expressing neurons over time, normalized by the initial value. In some experiments, cells were treated at time 0 (*arrow*) with 10 mM EGTA (*green*) or 50 μg/ml of soluble dimeric Nrx1β-Fc (*gray*). Traces are the averages of representative triplicate experiments. Curves in black represent simulations obtained with the following sets of parameters: Qdots Nrx1β, $\langle n \rangle = 5$; $k_{on} = 11\ min^{-1}$; $k_{off} = 0.9\ min^{-1}$; Qdots Nrx1β + EGTA, $\langle n \rangle = 5$; $k_{on} = 4\ min^{-1}$; $k_{off} = 1.2\ min^{-1}$; Qdots Nrx1β + soluble Nrx1β, $\langle n \rangle = 5$; $k_{on} = 7\ min^{-1}$; $k_{off} = 0.9\ min^{-1}$; and Qdots anti-HA, $\langle n \rangle = 10$; $k_{on} = 11\ min^{-1}$; $k_{off} = 0.6\ min^{-1}$.

around a mean value (Fig. 4 *b*). Nevertheless, one can unambiguously identify a long-term decrease in the number of Nrx1β-coated Qdots. In these conditions, the best fit of Nrx1β/Nlg1 detachment was obtained with $k_{on} = 8\ min^{-1}$ and $\langle n \rangle = 5$ (Fig. 4 *b* and Table 1). Diluting ligand concentration by a factor of 3 (1 Nrx1β-Fc molecule/1 QD) did not change the curve significantly (data not shown). Diluting even further (1 Nrx1β-Fc molecule/3 QD) resulted in a dramatic loss of binding to the cells, so the optimal ligand coating concentration lay in a fairly narrow range. As expected from a calcium-sensitive interaction, addition of EGTA to chelate extracellular calcium dramatically accelerated Qdot detachment (Fig. 4, *a* and *b*, and Movie S2). Control Qdots coated with anti-HA antibodies showed very little detachment in the same time frame (Fig. 4, *a* and *b*) and were not sensitive to EGTA (not shown). Addition of an excess of soluble Nrx1β to mobilize free Nlg-1 receptors resulted in a more rapid detachment of Nrx1β-coated Qdots (Fig. 4 *b*), confirming that this assay specifically probes the binding between Nrx1β and Nlg1.

Effects of ligand dimerization on receptor mobility and binding kinetics

We next examined the effects of ligand and receptor lateral associations on the kinetic rates of the Nrx1β/Nlg1 interaction. The use of the dimeric Nrx1β-Fc construct was anticipated to produce an approximate doubling of the number of Nrx1β ligands on each QD, since each anti-human binding site is likely to bind equally well to either monomeric or dimeric Fc. To get an indirect measurement of relative ligand number, we examined the lateral mobility of Qdots bound to monomeric or dimeric Nrx1β-Fc on the surface of neurons expressing Nlg1, after obtaining their individual 2D trajectory at high acquisition frequency (Fig. 5 *c*). The instantaneous diffusion coefficient calculated for populations of several hundreds of Qdots was widely distributed in the range 0–0.5 $\mu m^2/s$ (Fig. 5, *c* and *d*) for both conditions, but clearly revealed a difference between the two types of ligands. The average diffusion coefficient was 0.107 $\mu m^2/s$ for Qdots coated with monomeric Nrx1β-Fc and 0.077 $\mu m^2/s$ for Qdots coated with dimeric Nrx1β-Fc, suggesting that more receptors were being aggregated by Qdots bearing neurexin dimers. As expected from a larger amount of ligands, the detachment rate of Qdots coated with dimeric Nrx1β-Fc was much reduced compared with that of Qdots coated with monomeric Nrx1β-Fc (Fig. 6 *a*). The two experimental curves were fitted using the same k_{on} and k_{off} values, by considering $\langle n \rangle$ ligands for the monomeric Nrx1β-Fc, and $\langle 2n \rangle$ ligands for dimeric Nrx1β-Fc (Fig. 6 *a* and Table 1). The best agreement with the theoretical model was again obtained with $\langle n \rangle = 5$, consistent with our estimations of ligand number based on Fc-Cy3 fluorescence (Fig. 1, *c–e*) and Qdot mobility measurements (Fig. 5).

Effect of receptor dimerization and density on binding kinetics

Conversely, to characterize the impact of Nlg1 receptor dimerization on the binding to Nrx1β, we constructed and transfected a mutated Nlg1 receptor unable to form

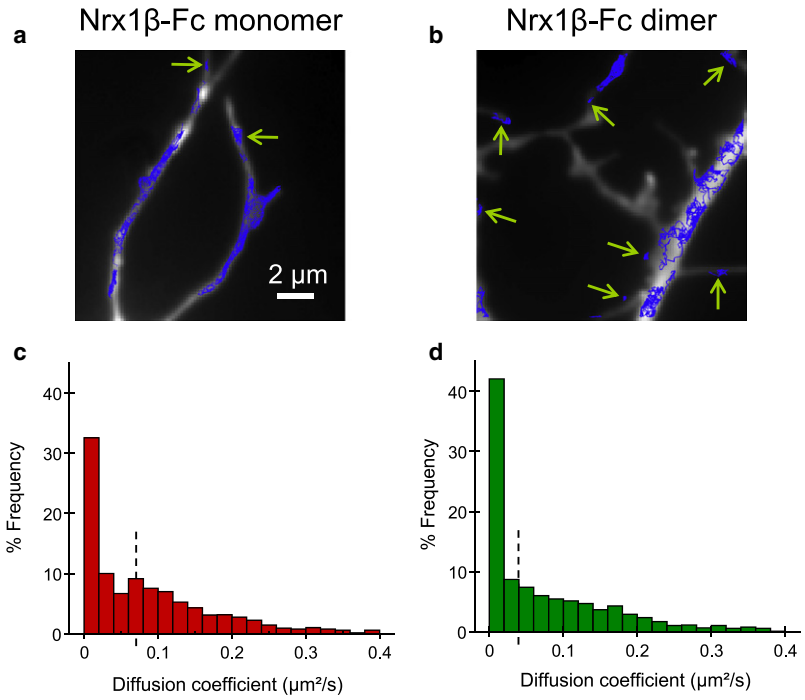

FIGURE 5 Effect of Nrx1β dimerization on the membrane diffusion of clustered Nlg1 receptors. (*a* and *b*) Qdots coated with either monomeric (*blue*) or dimeric Nrx1β-Fc (*red*) were incubated on neurons expressing wild-type Nlg1. The movements of Qdots were recorded at 30 Hz for 1 min and their individual trajectories (*blue*) were reconstructed as described and superimposed on the image of the Nlg1 + GFP transfected cell (*white*). Note a substantially higher fraction of slowly mobile Qdots for the Nrx1β dimer condition (*green arrows*). (*c* and *d*) The slope of the mean-square displacement versus time yielded the instantaneous diffusion coefficient, whose distribution is plotted for the two conditions. Numbers of Qdot trajectories were 1456 and 1079, respectively. Dashed lines indicate the medians of the distributions.

constitutive dimers. We compared the surface density of Nrx1β-Fc-coated Qdots bound to neurons transfected with either mutant or wild-type Nlg1 under identical labeling conditions and found similar values (0.32 ± 0.10, $n = 9$ cells, for the mutant, and 0.36 ± 0.05, $n = 20$ cells, for the wild-type), indicating that membrane expression was equally efficient for both molecules. In conditions of monomeric Nrx1β-Fc ligand coating, there was little difference in Qdot detachment between this mutant Nlg1-monomer and the wild-type counterpart (Fig. 6 *a* and Table 1). If anything, Nrx1β-Fc-coated Qdots detached less easily from mutated Nlg1 molecules, indicating a slightly higher k_{on} or lower k_{off}, or both.

Finally, we examined whether binding kinetics depended on the number of available receptors at the cell surface, which is directly related to the expression level of Nlg-1. We counted the number of Qdots bound to the cell at time 0, normalized by the projected cell area. Since experiments are reproducibly done with the same Qdot concentration and ligand density, this parameter should be proportional to the receptor density. By plotting k_{on} extracted from the fits with respect to Qdot density, we found a weak but significant correlation (Fig. 6 *b*), indicating that the binding rate is directly proportional to receptor concentration.

DISCUSSION

Pros and cons of the technique

We described here what to our knowledge is a novel technique based on tracking Qdot detachment, which stands as a convenient intermediate between single-molecule and population measurements. The behavior of ligand-coated Qdots reflects a history of random binding and unbinding events between ligands and receptors, with final detachment likely corresponding to the rupture of the last existing bond. Taking advantage of Qdot bleaching robustness, this assay is particularly suited for long-lasting interactions. It is also capable of detecting fast interactions by simply increasing the acquisition frequency, and thus applicable to virtually any type of biological interaction, provided one adapts ligand coating density to the specific kinetic parameters of each ligand/receptor pair. For very fast interactions or low ligand densities, one would have to implement a local application technique to detect quick detachment directly upon washout. A main advantage of this cell-based assay is that receptors can be manipulated using transfection or pharmacology. One could, for example, test the effect of intracellular adaptors and signaling pathways on the inside-out regulation of ligand-receptor affinity, as demonstrated for integrins. Also, by mutating protein domains involved in *cis*-oligomerization of IgCAMs or cadherins, one could selectively assess the effects of multivalency on the *trans*-binding of these proteins, as was done here for the neurexin/neuroligin complex. Another perspective would be to establish an image map of ligand/receptor affinity by computing local on/off rates on discrete surface regions, and to get information on cell membrane compartmentalization. However, one limitation concerns the reliance of adhesion proteins on homophilic binding. For example, in extracellular medium containing calcium, Qdots coated with molecules such as cadherins tend to aggregate instead of binding to the cells expressing the counter-receptors (not shown).

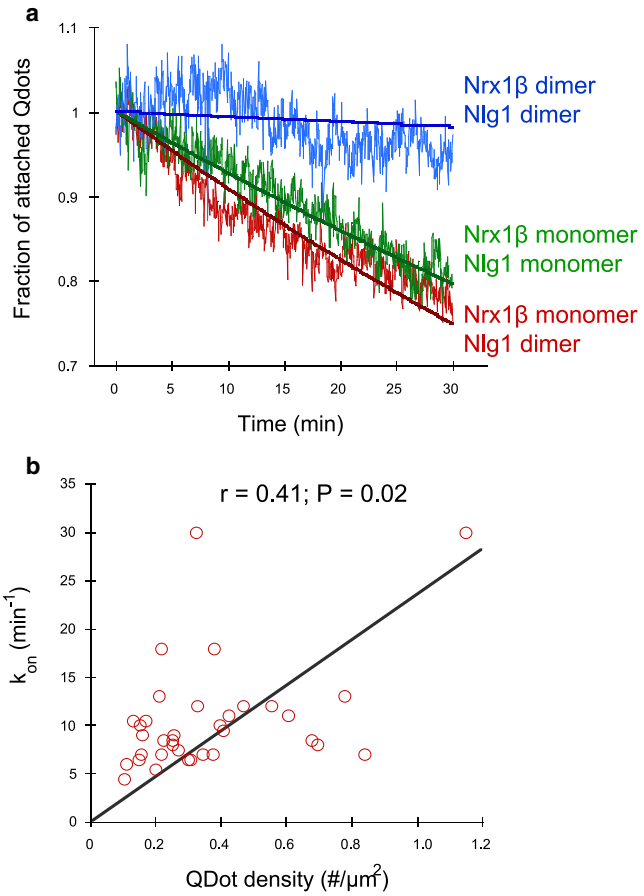

FIGURE 6 Effect of Nrx1β and Nlg1 dimerization on detachment kinetics. (*a*) Detachment of Qdots coated with either monomeric Nrx-1β (*red*) or dimeric Nrx-1β (*blue*) from Nlg1 expressing neurons was filmed for 30 min. The experimental traces are averages of 21 and 11 independent measurements, respectively. The solid lines are fits with $\langle n \rangle = 5$ and $\langle n \rangle = 10$, respectively, keeping $k_{on} = 11\ min^{-1}$ and $k_{off} = 0.9\ min^{-1}$ constant for both conditions. Alternatively, Qdots coated with monomeric Nrx1β-Fc were incubated on cells transfected with a mutant Nlg1 molecule unable to dimerize, Nlg1-monomer (*green*). The experimental trace is an average of nine independent measurements, and the solid line is a simulation with $\langle n \rangle = 5$, $k_{on} = 12\ min^{-1}$ and $k_{off} = 0.9\ min^{-1}$. (*b*) Relationship between calculated k_{on} and Qdot density on the cell surface, for all experiments using monomeric Nrx-1β. The correlation is significant, with a two-tailed *P* value of 0.02 using a nonparametric Spearman test ($r = 0.41$).

Comparison of kinetic parameters with other studies

When we fit the data of Qdot detachment with the kinetic model described above, we assigned a reasonable and fixed value to k_{off}, and computed k_{on} and $\langle n \rangle$ by comparing simulations with experimental curves. We took $k_{off} = 0.9\ min^{-1}$ from recent surface plasmon resonance experiments using soluble Nlg1 interacting with purified Nrx1β grafted onto flat substrates (5). Because the authors experienced difficulties in solubilizing the extracellular domain of wild-type Nlg1 (5), data are available only for mutant neuroligin molecules and various splice variants (5,12). Also, the fact that Nlg1 molecules are in solution may alter their binding properties when compared to our situation with membrane-anchored Nlg1. Thus, this k_{off} value is an initial guess that can be refined afterward. We initially considered k_{on} as a pooled parameter that implicitly included the global free receptor concentration, and we further showed that k_{on} was roughly proportional to receptor density, [R]. Thus, we can compute an intrinsic two-dimensional association rate by normalizing with receptor density: $K_{on} = k_{on}/[R]$, which is essentially the slope of the graph in Fig. 6 *b*. Assuming an average Nlg1 surface density around $500/\mu m^2$ (2,20), and taking $k_{on} = 10\ min^{-1}$, one obtains $K_{on} = 3 \times 10^{-4}\ \mu m^2/s$, very close to values reported for the integrin/fibronectin interaction (32). One also gets access to the two-dimensional $K_d = k_{off}/K_{on}$, on the order of $50\ \mu m^2$. For comparison, this is ~100 times lower than the E-selectin/carbohydrate ligand binding interaction (33), and 10-fold higher than K_d values measured in 2D semiartificial contacts for cell adhesion molecules implicated in the formation of the immunological synapse (1). The lifetime of the Nrx1β/Nlg1 interaction is also much larger than those of individual cadherin-cadherin (6) or selectin-carbohydrate interactions (7). This indicates that the neurexin/neuroligin complex provides long-lasting adhesion, in agreement with its physiological role of maintaining pre- together with postsynaptic compartments (14–16).

Effect of receptor oligomerization on diffusion and binding

We found a substantial reduction of Qdot diffusion upon coating with dimeric versus monomeric Nrx1β, in agreement with a viscous retardation of diffusion for particles aggregating more receptors. The actual relationship between the size of an object embedded in a two-dimensional fluid and its diffusion coefficient is complex and still a matter of debate. The seminal equation derived by Saffman and Delbrück based on the assumption of an ideal lipid bilayer (34) predicted a weak logarithmic dependence of diffusion coefficient on object radius. Some experimental data obtained both in living cells and artificial bilayers supported this model, at least for rather large objects (100 nm to 1 μm) (35–37). Other experiments on proteins embedded in liposomes (38), and mesoscopic simulations (39), suggest a much stronger dependence on object size, which may be due to local deformation of the membrane by protein/lipid interactions (40). For simplicity of analysis, we consider here that the diffusion coefficient scales as the inverse of the object radius, as predicted for small protein aggregates (38,40) Let us designate r as the radius of a neuroligin molecule, and $s = 4\pi r^2$ as the molecule's projected surface area. A cluster of n molecules has a projected area $S(n) = n \times s$, and thus a radius $R(n)$ equal to $r\sqrt{n}$. Hence, the ratio of diffusion coefficients between monomeric and dimeric Nrx1β-Fc coated Qdots should be $R(2n)/R(n) = \sqrt{2} = 1.41$. This value fits rather well with the experimental ratio between average diffusion coefficients, $0.107/0.077 = 1.38$, supporting the fact that Qdots coated with dimeric Nrx1β-Fc bear

TABLE 1 Summary of parameter values for the different conditions

Ligand coating	Nrx1β monomer	Nrx1β monomer	Nrx1β monomer + soluble Nrx1β	Nrx1β dimer
Receptor	Nlg1 monomer	Nlg1 dimer	Nlg1 dimer	Nlg1 dimer
k_{on} (min^{-1})	13.0 ± 3.2	13.1 ± 2.7*	8.8 ± 1.1*	13.6 ± 2.6
$\langle n \rangle$	5.9 ± 0.6	5.6 ± 0.6	4.8 ± 0.2	6.8 ± 0.5
No. of experiments	9	11	6	10

Due to some individual outliers, the average $\langle n \rangle$ values for Nrx1β monomers are somewhat higher, and the k_{on} values lower than those determined from the averaged detachment curve (see Figs. 4 *b* and 6 *a*). Also, the $\langle n \rangle$ for Nrx1β dimer is lower than for the averaged detachment curve due to imprecision in fitting the curves showing very little detachment.

*For the competition study, k_{on} is significantly lower than in the absence of treatment ($P = 0.01$ by unpaired Student's *t*-test).

on average two times more ligands than those with monomeric Nrx1β-Fc. However, this analysis is only an approximation given the large spread of diffusion coefficients in both conditions (which may be due to differences in the actual number of ligands grafted on each Qdot) and should not be taken as a way to discriminate between the various models of protein diffusion in membranes.

Based on the results using mutated monomeric neuroligin-1, the proximity between the two ectodomains of the Nlg1 molecule does not seem to have a strong impact on the binding to Nrx1β ligands. Given that the diffusion properties of Nlg1-monomer were similar to the wild-type Nlg1 (not shown), this suggests that fast short-range lateral diffusion of a monomeric Nlg1 moiety can easily compensate for the avidity effect allowed by the presence of a constitutive Nlg1 dimer (e.g., rebinding after bond breakage). As we showed earlier for IgCAM- and cadherin-mediated adhesions (2,20), the limiting step here is the ligand/receptor binding reaction (most likely involving the proper orientation of the neurexin and neuroligin molecules), and not membrane diffusion of receptors. The facts that k_{on} is positively correlated to Nlg-1 receptor density and addition of an excess Nrx1β ligands accelerates dissociation further support the notion of a reaction-limited regime (26,41).

SUPPORTING MATERIAL

A figure and movie legends are available at http://www.biophysj.org/biophysj/supplemental/S0006-3495(09)00914-X.

We thank C. Breillat, B. Tessier, D. Bouchet, and A. Frouin for molecular biology, neuronal cultures, and protein purification, P. Gonzales for technical help, V. Racine and J. B. Sibarita for the Multidimensional Image Analysis program, C. Poujol for the Qdot counting algorithm, M. Mondin for help on Qdot mobility analysis, and M. Bruchez, N. Rebola, and R. Frischknecht for helpful discussions.

We acknowledge financial support from the French Ministry of Research, Centre Nationale de la Recherche Scientifique, Conseil Régional Aquitaine, the Fondation pour la Recherche Medicale en France, and the Agence Nationale de la Recherche.

REFERENCES

1. Dustin, M. L., L. M. Ferguson, P. Y. Chan, T. A. Springer, and D. E. Golan. 1996. Visualization of CD2 interaction with LFA-3 and determination of the two-dimensional dissociation constant for adhesion receptors in a contact area. *J. Cell Biol.* 132:465–474.
2. Thoumine, O., M. Lambert, R. M. Mege, and D. Choquet. 2006. Regulation of N-cadherin dynamics at neuronal contacts by ligand binding and cytoskeletal coupling. *Mol. Biol. Cell.* 17:862–875.
3. Baksh, M. M., C. Dean, S. Pautot, S. Demaria, E. Isacoff, et al. 2005. Neuronal activation by GPI-linked neuroligin-1 displayed in synthetic lipid bilayer membranes. *Langmuir.* 21:10693–10698.
4. Pautot, S., H. Lee, E. Y. Isacoff, and J. T. Groves. 2005. Neuronal synapse interaction reconstituted between live cells and supported lipid bilayers. *Nat. Chem. Biol.* 1:283–289.
5. Comoletti, D., R. Flynn, L. L. Jennings, A. Chubykin, T. Matsumura, et al. 2003. Characterization of the interaction of a recombinant soluble neuroligin-1 with neurexin-1β. *J. Biol. Chem.* 278:50497–50505.
6. Perret, E., A. M. Benoliel, P. Nassoy, A. Pierres, V. Delmas, et al. 2002. Fast dissociation kinetics between individual E-cadherin fragments revealed by flow chamber analysis. *EMBO J.* 21:2537–2546.
7. Marshall, B. T., M. Long, J. W. Piper, T. Yago, R. P. McEver, et al. 2003. Direct observation of catch bonds involving cell-adhesion molecules. *Nature.* 423:190–193.
8. Bayas, M. V., A. Leung, E. Evans, and D. Leckband. 2006. Lifetime measurements reveal kinetic differences between homophilic cadherin bonds. *Biophys. J.* 90:1385–1395.
9. Merkel, R., P. Nassoy, A. Leung, K. Ritchie, and E. Evans. 1999. Energy landscapes of receptor-ligand bonds explored with dynamic force spectroscopy. *Nature.* 397:50–53.
10. Thoumine, O., P. Kocian, A. Kottelat, and J. J. Meister. 2000. Short-term binding of fibroblasts to fibronectin: optical tweezers experiments and probabilistic analysis. *Eur. Biophys. J.* 29:398–408.
11. Baumgartner, W., G. J. Schutz, J. Wiegand, N. Golenhofen, and D. Drenckhahn. 2003. Cadherin function probed by laser tweezer and single molecule fluorescence in vascular endothelial cells. *J. Cell Sci.* 116:1001–1011.
12. Comoletti, D., R. E. Flynn, A. A. Boucard, B. Demeler, V. Schirf, et al. 2006. Gene selection, alternative splicing, and post-translational processing regulate neuroligin selectivity for β-neurexins. *Biochemistry.* 45:12816–12827.
13. Reissner, C., M. Klose, R. Fairless, and M. Missler. 2008. Mutational analysis of the neurexin/neuroligin complex reveals essential and regulatory components. *Proc. Natl. Acad. Sci. USA.* 105:15124–15129.
14. Sudhof, T. C. 2008. Neuroligins and neurexins link synaptic function to cognitive disease. *Nature.* 455:903–911.
15. Dean, C., F. G. Scholl, J. Choih, S. DeMaria, J. Berger, et al. 2003. Neurexin mediates the assembly of presynaptic terminals. *Nat. Neurosci.* 6:708–716.
16. Heine, M., O. Thoumine, M. Mondin, B. Tessier, G. Giannone, et al. 2008. Activity-independent and subunit-specific recruitment of functional AMPA receptors at neurexin/neuroligin contacts. *Proc. Natl. Acad. Sci. USA.* 105:20947–20952.
17. Lambert, M., F. Padilla, and R. M. Mege. 2000. Immobilized dimers of N-cadherin-Fc chimera mimic cadherin-mediated cell contact formation: contribution of both outside-in and inside-out signals. *J. Cell Sci.* 113:2207–2219.

18. Breillat, C., O. Thoumine, and D. Choquet. 2007. Characterization of SynCAM surface trafficking using a SynCAM derived ligand with high homophilic binding affinity. *Biochem. Biophys. Res. Commun.* 359:655–659.
19. Groc, L., M. Lafourcade, M. Heine, M. Renner, V. Racine, et al. 2007. Surface trafficking of neurotransmitter receptor: comparison between single-molecule/quantum dot strategies. *J. Neurosci.* 27:12433–12437.
20. Thoumine, O., E. Saint-Michel, C. Dequidt, J. Falk, R. Rudge, et al. 2005. Weak effect of membrane diffusion on the rate of receptor accumulation at adhesive contacts. *Biophys. J.* 89:L40–L42.
21. Larson, D. R., W. R. Zipfel, R. M. Williams, S. W. Clark, M. P. Bruchez, et al. 2003. Water-soluble quantum dots for multiphoton fluorescence imaging in vivo. *Science.* 300:1434–1436.
22. Doose, S., J. M. Tsay, F. Pinaud, and S. Weiss. 2005. Comparison of photophysical and colloidal properties of biocompatible semiconductor nanocrystals using fluorescence correlation spectroscopy. *Anal. Chem.* 77:2235–2242.
23. Howarth, M., W. Liu, S. Puthenveetil, Y. Zheng, L. F. Marshall, et al. 2008. Monovalent, reduced-size quantum dots for imaging receptors on living cells. *Nat. Methods.* 5:397–399.
24. Bruchez, M. P. 2008. Quantum dots in living cells: where is progress needed? NanoObjects in Living Cells, Villeneuve d'Asq, France, September 1–4. Conference abstract.
25. Bell, G. I. 1978. Models for the specific adhesion of cells to cells. *Science.* 200:618–627.
26. Wank, S. A., C. DeLisi, and H. Metzger. 1983. Analysis of the rate-limiting step in a ligand-cell receptor interaction: the immunoglobulin E system. *Biochemistry.* 22:954–959.
27. Lauffenburger, D., and C. DeLisi. 1983. Cell surface receptors: physical chemistry and cellular regulation. *Int. Rev. Cytol.* 84:269–302.
28. Kaplanski, G., C. Farnarier, O. Tissot, A. Pierres, A. M. Benoliel, et al. 1993. Granulocyte-endothelium initial adhesion. Analysis of transient binding events mediated by E-selectin in a laminar shear flow. *Biophys. J.* 64:1922–1933.
29. Chesla, S. E., P. Selvaraj, and C. Zhu. 1998. Measuring two-dimensional receptor-ligand binding kinetics by micropipette. *Biophys. J.* 75:1553–1572.
30. Schmidt, C. E., T. Chen, and D. A. Lauffenburger. 1994. Simulation of integrin-cytoskeletal interactions in migrating fibroblasts. *Biophys. J.* 67:461–474.
31. Bruchez, M. P. 2005. Turning all the lights on: quantum dots in cellular assays. *Curr. Opin. Chem. Biol.* 9:533–537.
32. Thoumine, O., and J. J. Meister. 2000. Dynamics of adhesive rupture between fibroblasts and fibronectin: microplate manipulations and deterministic model. *Eur. Biophys. J.* 29:409–419.
33. Piper, J. W., R. A. Swerlick, and C. Zhu. 1998. Determining force dependence of two-dimensional receptor-ligand binding affinity by centrifugation. *Biophys. J.* 74:492–513.
34. Saffman, P. G., and M. Delbruck. 1975. Brownian motion in biological membranes. *Proc. Natl. Acad. Sci. USA.* 72:3111–3113.
35. Cicuta, P., S. L. Keller, and S. L. Veatch. 2007. Diffusion of liquid domains in lipid bilayer membranes. *J. Phys. Chem. B.* 111:3328–3331.
36. Kucik, D. F., E. L. Elson, and M. P. Sheetz. 1999. Weak dependence of mobility of membrane protein aggregates on aggregate size supports a viscous model of retardation of diffusion. *Biophys. J.* 76:314–322.
37. Petrov, E. P., and P. Schwille. 2008. Translational diffusion in lipid membranes beyond the Saffman-Delbruck approximation. *Biophys. J.* 94:L41–L43.
38. Gambin, Y., R. Lopez-Esparza, M. Reffay, E. Sierecki, N. S. Gov, et al. 2006. Lateral mobility of proteins in liquid membranes revisited. *Proc. Natl. Acad. Sci. USA.* 103:2098–2102.
39. Guigas, G., and M. Weiss. 2006. Size-dependent diffusion of membrane inclusions. *Biophys. J.* 91:2393–2398.
40. Naji, A., A. J. Levine, and P. A. Pincus. 2007. Corrections to the Saffman-Delbruck mobility for membrane bound proteins. *Biophys. J.* 93:L49–L51.
41. DeLisi, C., and R. Chabay. 1979. The influence of cell surface receptor clustering on the thermodynamics of ligand binding and the kinetics of its dissociation. *Cell Biophys.* 1:117–131.